An Implicit Solver For 1D Arterial Network Models

Jason Carson[1] and Raoul Van Loon[1]

[1]*Zienkiewicz Centre for Computational Engineering, College of Engineering, Swansea University, Bay Campus, Fabian Way, Swansea, SA1 8EN.*

Abstract

In this study the one dimensional blood flow equations are solved using a newly proposed enhanced trapezoidal rule method ETM, which is an extension to the simplified trapezoidal rule method STM. At vessel junctions the conservation of mass and conservation of total pressure are held as system constraints using Lagrange multipliers that can be physically interpreted as external flow rates. The ETM scheme is compared with published arterial network benchmark problems and a dam break problem. Strengths of the ETM scheme include being simple to implement, intuitive connection to lumped parameter models, and no restrictive stability criteria such as the CFL number. The ETM scheme does not require the use of characteristics at vessel junctions, or for inlet and outlet boundary conditions. The ETM forms an implicit system of equations which requires only one global solve per time step for pressure, followed by flow rate update on the elemental system of equations, thus no iterations are required per time step. Consistent results are found for all benchmark cases and for a 56 vessel arterial network problem it gives very satisfactory solutions at a spatial and time discretisation that results in a maximum CFL of 3, taking 4.44 seconds per cardiac cycle. By increasing the time step and element size to produce a maximum CFL number of 15 the method takes only 0.39 seconds per cardiac cycle with only a small compromise on accuracy.

Keywords: 1D arterial network; implicit solvers; finite elements; lumped models; Lagrange multipliers; penalty method

1 Introduction

One-dimensional blood flow models have become more and more recognised as a powerful tool for the analysis of pressure and flow pulses in the cardiovascular system. These 1D models use relatively simple (non-)linear relation between pressure in the vessel and area (constitutive law), and simplified velocity profiles. If localised flow fields are not of interest, one-dimensional models can be a computationally inexpensive alternative to three-dimensional fluid-structure interaction models.

Important contributions to the development of 1D models include studies by Hughes and Lubliner [1], Stergiopoulos [2], Stergiopoulos *et al.* [3], Olufsen *et al.* [4], Formaggia *et al.* [5], Hellevik *et al.* [6], Bessems *et al.* [7], Sherwin *et al.* [8], Mynard and Nithiarasu [9], Müller and Toro [10, 11, 12], Low *et al.* [13] and, Blanco *et al.* [14, 15, 16]. There have also been methods proposed

†Email: R.VanLoon@swansea.ac.uk

for 1D-3D coupling [14, 17, 18, 19] and a semi-implicit method that allows 1D or 2D simulations within the same framework [20]. Models concentrating on specific vessels have been proposed such as the arm [21], the calf muscle [22], carotid artery [23], cerebral circulation [24], foetal veins [25], neonatal pulmonary atresia [26], valve models [27]. Inlet boundary conditions used in these models may also include a heart model with cardiac valves [9, 13, 11, 12]. Mynard and Smolich [28] presented a fully closed system, incorporating a heart model with chamber interactions, coronary model with interaction from the heart, with 1D vessels for both systemic and pulmonary arteries and veins. There are various outlet (terminal) boundary conditions such as structured tree models [4], simple resistance models or Windkessel models [29].

Many different formulations have been proposed and various numerical methods have been developed. As the equations govern non-linear wave propagations, these cardiovascular flow problems are typically solved using shock capturing numerical schemes, like Discontinuous Galerkin and Taylor-Galerkin in finite elements or high-resolution finite volume methods and finite difference methods. However, under normal physiological conditions shocks do not appear in the arterial system.

Wang *et al.* [30] compared four numerical schemes which included the local discontinuous Galerkin, MacCormack, Taylor-Galerkin and monotonic upwind scheme for conservation laws (MUSCL). These comparisons were tested on a single vessel, a simple bifurcation and an arterial network comprising of 55 arteries. The conclusions from [30] indicated that the MacCormack scheme was best in cases of small non-linearities as it is robust and very simple to implement. The second order finite volume scheme (MUSCL) was a better option when there were shock like phenomena present. Taylor-Galerkin had a good balance between speed and accuracy if no shock phenomena were present. The local discontinuous Galerkin method was suitable for systems with a small physical diffusive term. Recently a benchmark paper by Boileau *et al.* [31] included cases which had experimental and 3D data for comparing accuracy. There were six numerical schemes that were compared. These were: locally conservative Galerkin (LCG) [9], discontinuous Galerkin (DCG) [32], Galerkin least-squares finite element method (FEM) [14], finite volume method (FVM) [11, 12], finite difference method MacCormack (McC) [25], and, the Simplified Trapezoidal Method (STM) [33]. There were six test cases which ranged from single vessels (single reflection free tube, common carotid artery and upper thoracic aorta), a bifurcation (aortic bifurcation) and two different arterial networks (one with 37 arteries and the other with 56). The results for 5 of the cases were consistent amongst all schemes. However, in the 56 arterial network (ADAN56) the results from the STM scheme deviated from the results of other methods.

The aim of this paper is to develop an implicit scheme for 1D blood flow to alleviate CFL restrictions and prevent non-linear solves for the characteristics at vessel junctions. Lagrange multipliers and penalty methods will be used to hold the system constraints in place at vessel junctions to prevent using characteristics. The scheme is tested on all the benchmark test problems presented in [31]. These tests include: a single pulse in a reflection free tube to which a theoretical solution exists, a common carotid artery, an upper thoracic aorta, an aortic bifurcation, a 37-arterial tree network with experimental data, and a 56-arterial tree model. Although physiologically not very common, performance of the ETM scheme is also explored for shock waves.

2 One Dimensional Blood Flow Model

There are various formulations for the 1D blood flow equations. The AU (area and average axial velocity) [9, 32]; AQ (area and average flow rate) [10, 11, 12, 5]; PQ (pressure and average flow rate) [7, 33]; and in characteristic variables [15]. The model presented here is equivalent to the model described in [31]. In the one dimensional model the arteries are split into a number of segments connected at nodes. Each segment is considered as a deformable tube, which represents a blood vessel. Due to various assumptions, the system can be modelled using a single axial coordinate x. The wall of the vessel is considered impermeable and blood is assumed to be an incompressible Newtonian fluid. The system of equations that describes blood flow in major arteries in PQ form is given by the conservation of mass and the conservation of momentum

$$\begin{cases} C_A \frac{\partial P}{\partial t} + \frac{\partial Q}{\partial x} = 0, \\ \\ \frac{\rho}{A}\frac{\partial Q}{\partial t} + \frac{\rho}{A}\frac{\partial}{\partial x}\left(\frac{Q^2}{A}\right) + \frac{\partial P}{\partial x} - \frac{f}{A} = 0, \end{cases} \tag{1}$$

where t is the time; $Q(x,t)$ is the average flow rate in the cross-section; $P(x,t)$ is the average pressure in the cross-section; $A(x,t)$ is the cross-sectional area; ρ is the blood density; $f(x,t)$ is the frictional force per unit length; and C_A is the vessel compliance given by

$$C_A = \frac{\partial A}{\partial P} = \left(\frac{2A_d\left(P - P_{ext} - P_d\right)}{\beta} + 2\sqrt{A_d}\right)\frac{A_d}{\beta}. \tag{2}$$

The relationship between pressure and area (constitutive law) which accounts for the fluid-structure interaction of the system is

$$P = P_{ext} + P_d + \frac{\beta}{A_d}\left(\sqrt{A} - \sqrt{A_d}\right), \quad \beta(x) = 4/3\sqrt{\pi}Eh, \tag{3}$$

where P_{ext} is the external pressure; $P_d(x)$ and $A_d(x)$ are the diastolic pressure and area respectively; $\beta(x)$ accounts for material properties where $E(x)$ and $h(x)$ are the elastic modulus and wall thickness respectively. The velocity profile is chosen as

$$u(x,\xi,t) = U(x,t)\frac{\xi+2}{\xi}\left[1 - \left(\frac{\xi}{r}\right)^{\zeta}\right], \tag{4}$$

where $u(x,\xi,t)$ is the axial velocity profile; $U = Q/A$ is the average axial velocity in the cross-section; ξ is a radial coordinate; r(x,t) is the lumen radius; ζ is a given constant for a specific profile. This means the frictional force becomes

$$f = -2(\zeta+2)\mu\pi\frac{Q}{A}, \tag{5}$$

where μ is the dynamic viscosity.

2.1 Boundary Conditions

To validate our method a comparison is performed with several benchmark problems as proposed in Boileau *et al.* [31], so the same boundary conditions will be applied in this work, unless stated otherwise. Therefore, a flow rate is prescribed as the inlet boundary condition for the common carotid artery (Section 4.4), upper thoracic aorta (Section 4.5), aortic bifurcation (Section 4.6), 37-arterial tree (Section 4.7) and ADAN56 arterial network (Section 4.8) problems. The outlet of the arterial system model is connected to a 3-element Windkessel model (or single resistance model), which comprises of a resistor R_1 (characteristic impedance) in series with a resistor R_2 (peripheral resistance) and capacitor C (Compliance) in parallel. This is normally calculated using the single differential equation

$$Q\left(1+\frac{R_1}{R_2}\right)+CR_1\frac{\partial Q}{\partial t}=\frac{P-P_{out}}{R_2}+C\frac{\partial P}{\partial t}. \tag{6}$$

The majority of schemes such as those in [9, 32, 25, 11], use characteristic equations at the inlet and use both characteristic equations together with Equation (6) and Newton-Raphson iterations to determine variables at the outlet. It is also possible to separate this differential equation into its individual components. This would include two resistance elements and a compliance element. This will be discussed further in Section 3.1.

3 Numerical Methods

3.1 Enhanced Trapezoidal Method

The ETM scheme is an extension to the method proposed by Kroon *et al.* [33]. The method was called simplified trapezoidal rule method (STM) in the paper by Boileau *et al.* [31]. An important property of the method is that all flows Q are directed inwards (toward the element centre), which has major implications when implementing the method. The scheme can be derived by using the trapezoidal rule in space on the elemental blood flow equations with a particular manipulation of the flow rates, assuming $\zeta = 2$ during the formulation. The system of equations in a PQ formulation is given by Equation (1). The equations are linearised (see [33] for more details) in the following way

$$C_a^{n+1}\approx C_a^{n+1,k},\quad Q^{n+1}\approx Q^{n+1,k+1},\quad P^{n+1}\approx P^{n+1,k+1},$$

$$\frac{Q^2}{A}^{n+1}\approx\frac{Q^2}{A}^{n+1,k},\quad \frac{\rho}{A}^{n+1}\approx\frac{\rho}{A}^{n+1,k},\quad \left(\frac{8\mu\pi Q}{A^2}\right)^{n+1}\approx\left(\frac{8\mu\pi Q}{A^2}\right)^{n+1,k}, \tag{7}$$

where superscript k is the iteration level, and as an initial guess $k = 1 \approx n$. However, in this paper no iterations are performed, which means $(n+1,k)\approx(n)$ and $(n+1,k+1)\approx(n+1)$. The linearised system then has the form

$$C_A^n\frac{\partial P}{\partial t}+\frac{\partial Q^{n+1}}{\partial x}=0, \tag{8}$$

$$\frac{\rho}{A^n}\frac{\partial Q}{\partial t}+\frac{\partial P^{n+1}}{\partial x}=\left(-\frac{8\mu\pi Q}{A^2}-\frac{\rho}{A}\frac{\partial(\frac{Q^2}{A})}{\partial x}\right)^n, \tag{9}$$

where Equations (8) and (9) are the conservation of mass and momentum respectively. The domain is then split into smaller elements with 2 nodes each. This system is integrated in space using the trapezoidal rule. Looking at each term individually and integrating the mass equation within an element gives

$$\int_e \left(C_A^n \frac{\partial P}{\partial t} \right) dx = \frac{\Delta x}{2} \left(C_{A,1}^n \frac{\partial P_1}{\partial t} + C_{A,2}^n \frac{\partial P_2}{\partial t} \right), \tag{10}$$

$$\int_e \left(\frac{\partial Q^{n+1}}{\partial x} \right) dx = \left(Q_2^{n+1} - Q_1^{n+1} \right). \tag{11}$$

In a similar way for conservation of momentum

$$\int_e \left(\frac{\rho}{A^n} \frac{\partial Q}{\partial t} \right) dx = \frac{\Delta x}{2} \left(\frac{\rho}{A_1^n} \frac{\partial Q_1}{\partial t} + \frac{\rho}{A_2^n} \frac{\partial Q_2}{\partial t} \right). \tag{12}$$

The second term of the conservation of momentum is

$$\int_e \left(\frac{\partial P^{n+1}}{\partial x} \right) dx = \left(P_2^{n+1} - P_1^{n+1} \right). \tag{13}$$

Letting the right side of Equation (9) be

$$h = \left(\frac{-8\pi\mu Q}{A^2} - \frac{\rho}{A} \frac{\partial \left(\frac{Q^2}{A} \right)}{\partial x} \right)^n. \tag{14}$$

Integrating gives

$$\int_e (h)^n dx = \frac{\Delta x}{2} \left(h_1 + h_2 \right)^n. \tag{15}$$

This indicates that the mass and momentum is conserved at the element centre, while the variables are defined on the nodes. Using second order backward difference for the time derivatives ($\frac{\partial U}{\partial t} \approx \frac{3}{2\Delta t} U^{n+1} - \frac{2}{\Delta t} U^n + \frac{1}{2\Delta t} U^{n-1}$) gives the system in the exact same form as Kroon *et al.* [33].

$$\begin{bmatrix} \frac{3}{2\Delta t} \frac{\Delta x}{2} C_{A,1}^n, & \frac{3}{2\Delta t} \frac{\Delta x}{2} C_{A,2}^n \\ -1, & 1 \end{bmatrix} \begin{bmatrix} P_1 \\ P_2 \end{bmatrix}_e^{n+1} + \begin{bmatrix} -1, & 1 \\ \frac{3}{2\Delta t} \frac{\Delta x}{2} \frac{\rho}{A_1^n}, & \frac{3}{2\Delta t} \frac{\Delta x}{2} \frac{\rho}{A_2^n} \end{bmatrix} \begin{bmatrix} Q_1 \\ Q_2 \end{bmatrix}_e^{n+1}$$
$$= \begin{bmatrix} 0 \\ \frac{\Delta x}{2} (h_1^n + h_2^n) \end{bmatrix}_e + \begin{bmatrix} \frac{\Delta x}{2} \left(C_A^n \frac{2}{\Delta t} P^n - C_A^n \frac{1}{2\Delta t} P^{n-1} \right)_1 \\ \frac{\Delta x}{2} \left(\frac{\rho}{A^n} \frac{2}{\Delta t} Q^n - \frac{\rho}{A^n} \frac{1}{2\Delta t} Q^{n-1} \right)_1 \end{bmatrix}_e + \begin{bmatrix} \frac{\Delta x}{2} \left(C_A^n \frac{2}{\Delta t} P^n - C_A^n \frac{1}{2\Delta t} P^{n-1} \right)_2 \\ \frac{\Delta x}{2} \left(\frac{\rho}{A^n} \frac{2}{\Delta t} Q^n - \frac{\rho}{A^n} \frac{1}{2\Delta t} Q^{n-1} \right)_2 \end{bmatrix}_e$$

which can be generalised to

$$\boldsymbol{F}_e \boldsymbol{P}_e^{n+1} + \boldsymbol{G}_e^c \boldsymbol{Q}_e^{c,n+1} = \boldsymbol{h}_e^n. \tag{16}$$

where superscript c represents conventional discretisation (before flows are directed inwards) and subscript e represents the elemental level.

The second term on the right side of Equation (14) uses the following first order upwind discretisation for node i to avoid spatial oscillations that would occur from central differencing. For

two neighbouring elements that share node i

$$\frac{\partial \left(\frac{Q^2}{A}\right)^n}{\partial x} \approx \begin{cases} \left[\left(\frac{Q^2}{A}\right)_i - \left(\frac{Q^2}{A}\right)_{i-1}\right] \frac{1}{\Delta x} & \text{if} \quad Q_i^n > 0, \\ \left[\left(\frac{Q^2}{A}\right)_{i+1} - \left(\frac{Q^2}{A}\right)_i\right] \frac{1}{\Delta x} & \text{if} \quad Q_i^n < 0, \end{cases} \tag{17}$$

where node $i-1$ would be the first node of element 1, node i is the second node in element 1 and the first node in element 2, while node $i+1$ would be the second node in element 2. If required a ghost node is used at the vessel boundaries. At this point the flows are enforced to be directed inwards (defined to point towards element centre) which implies changing the sign of the second row of $\boldsymbol{Q}_e^c$ (Q at second node) and changing the sign of the second column of the matrix $\boldsymbol{G}_e^c$.

$$\boldsymbol{G}_e^c = \begin{bmatrix} G_{11} & G_{12} \\ G_{21} & G_{22} \end{bmatrix}, \quad \text{becomes} \quad \boldsymbol{G_e} = \begin{bmatrix} G_{11} & -G_{12} \\ G_{21} & -G_{22} \end{bmatrix}. \tag{18}$$

While flows $Q_e^c = \begin{bmatrix} Q_1, Q_2 \end{bmatrix}^T$ become $Q_e = \begin{bmatrix} Q_1, -Q_2 \end{bmatrix}^T$. This means that the system equations will still be the same as before when multiplied out. Matrix $\boldsymbol{G_e}$ is then inverted so the final elemental system of equations is given by

$$[-\boldsymbol{G_e}^{-1}\boldsymbol{F}_e]\boldsymbol{P}_e^{n+1} = [-\boldsymbol{G_e}^{-1}\boldsymbol{h}_e^n] + \boldsymbol{Q}_e^{n+1}. \tag{19}$$

Once these elemental systems are assembled into the global system matrix it can be seen that the flow column $\boldsymbol{Q}_g^{n+1}$ becomes the conservation of mass between connected elements and hence is zero for all internal nodes. The flow column then only has non-zero values on the boundaries, which represent external flows. That is $\boldsymbol{Q}_g^{n+1} = \begin{bmatrix} Q_{inflow}, 0, \ldots, 0, Q_{outflow} \end{bmatrix}$. This has major implications on the implementation at junctions, such as bifurcations, as the continuity of mass is automatically satisfied. Moreover, the STM scheme uses the same pressure node (last node in parent and first nodes in daughters) such that the conservation of static pressure is also satisfied. Hence, no additional constraints need to be applied (see [33] for full details on the STM method).

However, this limits the STM method as only conservation of static pressure can be imposed. Therefore the ETM method extends the existing STM method to allow conservation of total pressure to be applied between vessel segments, whilst within a vessel segment the ETM and STM are identical. This difference only occurs at vessel junctions as will be discussed in Section 3.2. Once the global matrix is assembled the implicit system is solved for pressures, then the flows can be updated using the elemental system (19).

As an example of two neighbouring elements within the same vessel, let

$$[-\boldsymbol{G_e}^{-1}\boldsymbol{F}_e] = \boldsymbol{K}_e, \quad \text{and} \quad [-\boldsymbol{G_e}^{-1}\boldsymbol{h}_e^n] = \boldsymbol{f}_e. \tag{20}$$

which means Equation (19) takes the form

$$\boldsymbol{K}_e\boldsymbol{P}_e^{n+1} = \boldsymbol{f}_e^n + \boldsymbol{Q}_e^{n+1}, \tag{21}$$

where

$$\boldsymbol{K}_e = \begin{bmatrix} K_{11}^e & K_{12}^e \\ K_{21}^e & K_{22}^e \end{bmatrix}, \quad \boldsymbol{f}_e^n = \begin{bmatrix} f_1 \\ f_2 \end{bmatrix}, \tag{22}$$

and $\boldsymbol{P}_e^{n+1} = \begin{bmatrix} P_1 & P_2 \end{bmatrix}^T$, $\boldsymbol{Q}_e^{n+1} = \begin{bmatrix} Q_1 & -Q_2 \end{bmatrix}^T$. Consider element one with pressure nodes P_1 and P_2 and flows Q_1 and Q_2, and element two with pressure nodes P_2 and P_3 and flows Q_3 and Q_4 respectively. Assembling these two elemental system leads to the following system,

$$\begin{bmatrix} K_{11}^1 & K_{12}^1 & 0 \\ K_{21}^1 & K_{22}^1 + K_{11}^2 & K_{12}^2 \\ 0 & K_{21}^2 & K_{22}^2 \end{bmatrix} \begin{bmatrix} P_1 \\ P_2 \\ P_3 \end{bmatrix}^{n+1} = \begin{bmatrix} f_1^1 \\ f_1^2 + f_2^1 \\ f_2^2 \end{bmatrix} + \begin{bmatrix} Q_1 \\ -Q_2 + Q_3 \\ -Q_4 \end{bmatrix}^{n+1}. \tag{23}$$

where the superscripts on K and f represent which element they belong to. The conservation of mass between element one and two requires the outflow of element one (Q_2) to be equal to inflow of element two (Q_3), hence $Q_2 = Q_3$ or rearranged $0 = Q_3 - Q_2$. This is exactly the middle value in the flow column (last term on right) in Equation (23). Thus only inflow Q_1 and outflow Q_4 (boundary conditions) of this column vector are non-zero, at which either pressure or flow rate would be prescribed. This implicit use of conservation of mass occurs when: 1D elements connect with other 1D elements; when 1D elements connect to one, or multiple lumped (0D) elements; and when any number of lumped elements connects to any number of other 0D elements.

The inlet boundary condition for the benchmark problems is given as a flow rate, which is easily implemented in the STM and ETM methods using the external flow column vector $\boldsymbol{Q}_g^{n+1}$. If the pressure is required as a boundary condition then this can be imposed as a Dirichlet boundary condition.

The outlet of the arterial system model is connected to a 3-element Windkessel model, which comprises of a resistor R_1 (characteristic impedance) in series with a resistor R_2 (peripheral resistance) and capacitor C (compliance) in parallel. This is normally calculated using the single differential equation (6).

However, following the approach by Kroon *et al.* [33] the Windkessel model can be treated using the basic element equations with two pressure nodes and two flow rate nodes given by

$$\frac{1}{R_1}(P_1^{n+1} - P_2^{n+1}) = q_1^{n+1} = -q_2^{n+1}; \tag{24}$$

$$\frac{1}{R_2}(P_2^{n+1} - P_3^{n+1}) = q_3^{n+1} = -q_4^{n+1}; \tag{25}$$

$$C(\frac{\partial P_2}{\partial t} - \frac{\partial P_4}{\partial t}) = q_5^{n+1} = -q_6^{n+1}; \tag{26}$$

Note that the flow rates for nodes one and two q_1, q_2 have opposite signs due to the requirement that flow rates are defined inwards towards the element centre. The temporal term in Equation (26) is once again descretised by a second order backward difference scheme. The elemental Windkessel equations have the same form as the 1D blood flow equations with pressure being the only unknown variable.

$$\boldsymbol{K}_e^{0D} \boldsymbol{P}_e^{n+1} = \boldsymbol{f_e} + \boldsymbol{Q}_e^{n+1}. \tag{27}$$

Like for the 1D equations the flow rate column once again becomes zero (conservation of mass) in internal nodes with only external flows being non-zero after assembly of the elemental Windkessel equations. This also allows the Windkessel model to be easily connected to the 1D blood flow equations, where once again the conservation of mass appears in the flow rate column. For more details on the implementation see [33]. The outlet boundary condition for the Windkessel is a pressure, which is applied to the system matrix directly. The flow rate could be given in which case the boundary condition would simply be added to the flow rate vector, $\boldsymbol{Q}^{n+1}$.

3.2 Vessel To Vessel Interface Conditions

In many works [9, 32, 25, 11] characteristics are used along with conservation of mass and conservation of total pressure at vessel junctions. A Newton-Raphson method is then used to update variables to provide boundary conditions of the vessels at the next time step. This needs to be performed at every vessel junction and could be very expensive depending on how many junctions are considered.

In this paper interface constraints are held in place using either Lagrange multipliers or the penalty method (see [34] for more details on their implementation). To implement Lagrange multipliers first consider the system of equations representing 1D blood flow written in the form $\boldsymbol{Ax} = \boldsymbol{b}$, which are subject to constraints at an interface between vessels. If we consider N number of vessels at a junction then the system of equations needs to be supplemented with N constraints g_1 and g_i. The constraints are given by the continuity of mass (g_1) and continuity of total pressure (g_i $i = 2, \ldots, N$)

$$g_1 = \sum_{i=1}^{N} Q_i = 0, \tag{28}$$

$$g_i = \frac{\rho}{2}\frac{Q_1^2}{A_1^2} + P_1 - \frac{\rho}{2}\frac{Q_i^2}{A_i^2} - P_i = 0, \qquad i = 2, \ldots, N. \tag{29}$$

where subscript 1 is the chosen reference vessel. These constraints are imposed for the time level $n + 1$ and hence need to be linearised. After linearisation the constraints for all junctions can be combined into the system $\boldsymbol{Bx} = \boldsymbol{c}$, which is the same form as the blood flow equations.

At each junction there are N equations which need to be satisfied at the interface between the parent and N daughter vessels, implying that N Lagrange multipliers will be needed to impose these constraints at each vessel junction. For the global system, the Lagrange multipliers for all vessel junctions are given by $\lambda_{1,\ldots,M}$. Where M is the total number of Lagrange multipliers needed to constrain conservation of mass and conservation of total pressure at all vessel junctions. These can be added to the system of equations in the following way. Let $\boldsymbol{\Lambda}$ be a vector containing all $\lambda_{1,\ldots,M}$, consider

$$\boldsymbol{\Lambda}^T(\boldsymbol{Bx} - \boldsymbol{c}) = 0. \tag{30}$$

Defining an energy functional as

$$\delta I = (\boldsymbol{Ax} - \boldsymbol{b})^T \delta x = \delta(\boldsymbol{x}^T \boldsymbol{Ax} - \boldsymbol{x}^T \boldsymbol{b}). \tag{31}$$

where $\boldsymbol{Ax} - \boldsymbol{b}$ are the system of equations which model blood flow. The stationary condition that

satisfies this is

$$I = (\boldsymbol{x}^T \boldsymbol{A}\boldsymbol{x} - \boldsymbol{x}^T \boldsymbol{b}). \tag{32}$$

Creating a functional by adding Equations (32) and (30) gives

$$J = \boldsymbol{x}^T \boldsymbol{A}\boldsymbol{x} - \boldsymbol{x}^T \boldsymbol{b} + \boldsymbol{\Lambda}^T (\boldsymbol{B}\boldsymbol{x} - \boldsymbol{c}). \tag{33}$$

Requiring that the total variation of this functional $\delta J = 0$.

$$\delta J = \frac{\partial J}{\partial x_i}\delta x_i + \frac{\partial J}{\partial \lambda_i}\delta \lambda_i = 0. \tag{34}$$

Implies that

$$\frac{\partial J}{\partial x_i} = 0, \qquad \text{and} \qquad \frac{\partial J}{\partial \lambda_i} = 0, \tag{35}$$

as δx_i and $\delta \lambda_i$ are arbitrary. Thus the full system to be solved can be written as

$$\begin{bmatrix} \boldsymbol{A} & \boldsymbol{B}^T \\ \boldsymbol{B} & \boldsymbol{0} \end{bmatrix} \begin{bmatrix} \boldsymbol{x} \\ \Lambda \end{bmatrix} = \begin{bmatrix} \boldsymbol{b} \\ \boldsymbol{c} \end{bmatrix} \tag{36}$$

The penalty method is an alternative option to the use of Lagrange multipliers. The penalty method turns a constrained problem into an unconstrained problem. The theory also comes from calculus of variations. Consider the system energy functional as Equations (31) and (32). The problem involves finding the stationary points of the functional I subjected to constraints. The system has constraints which can be written in the form $\boldsymbol{C} = \boldsymbol{B}\boldsymbol{x} - \boldsymbol{c}$ [34], where $\boldsymbol{C}$ will effectively be a column vector of residuals C_i for ($i = 1, \cdots N_{constraints}$). Any entry in the vector $\boldsymbol{C}$ that is not zero implies that the constraint is not satisfied. Pre-multiplying this column vector with its transpose gives

$$\boldsymbol{C}^T \boldsymbol{C} = C_1^2 + C_2^2 + \cdots + C_{N_{constraints}}^2. \tag{37}$$

When $\boldsymbol{C}^T \boldsymbol{C} = 0$ the constraints are satisfied and also the variation $\delta(\boldsymbol{C}^T \boldsymbol{C}) = 0$. Creating a new functional

$$J = I + \frac{1}{2}\alpha \boldsymbol{C}^T \boldsymbol{C}, \tag{38}$$

where α is a penalty number. The solution of the unconstrained system will be to find the stationary point of the energy functional J which is when $\delta J = 0$. The solution of this stationary point of J will only approximately satisfy the constraints of the system. The larger the value of α the more accurately the constraints will be imposed.

In order to apply the penalty method consider the system of equations that needs to be solved written in the form $\boldsymbol{A}\boldsymbol{x} = \boldsymbol{b}$. This system is subjected to boundary conditions which are written in the form $\boldsymbol{B}\boldsymbol{x} = \boldsymbol{c}$. Applying the penalty method will lead to the system of equations that is to be solved as

$$(\boldsymbol{A} + \boldsymbol{B}^T \boldsymbol{\alpha} \boldsymbol{B})\boldsymbol{x} = \boldsymbol{b} + \boldsymbol{B}^T \boldsymbol{\alpha} \boldsymbol{c}. \tag{39}$$

where $\boldsymbol{\alpha}$ is a diagonal matrix containing all α_i. Note that if all values α_i are equal then this diagonal matrix can be replaced by a single value α, which is the approach used in this paper.

As mentioned previously the interface conditions used in the STM model are the conservation

of mass and the conservation of static pressure. This use of static pressure, rather than total pressure led to a decrease in the scheme's performance in the ADAN56 arterial tree, when compared to results of other schemes (see [31] for details). Moreover, as the STM method implicitly applies the conservation of static pressure in the formulation, it is not straightforward to include the dynamic pressure. Other schemes can choose which interface conditions to apply, usually imposing them along with continuity of the Riemann invariants.

In order to use Lagrange multipliers to hold conservation of total pressure as a constraint, a separation of pressure nodes at vessel junctions is required. In the method by Kroon *et al.* [33] only one pressure node is present at the bifurcation while now there are three (corresponding to the outlet of the parent vessel and the inlets of both daughter vessels) as shown in Figure 1. Moreover, mass conservation does not need to be explicitly constrained as it will automatically be satisfied when conservation of total pressure is applied via Lagrange multipliers, this will be discussed in Section 3.3.

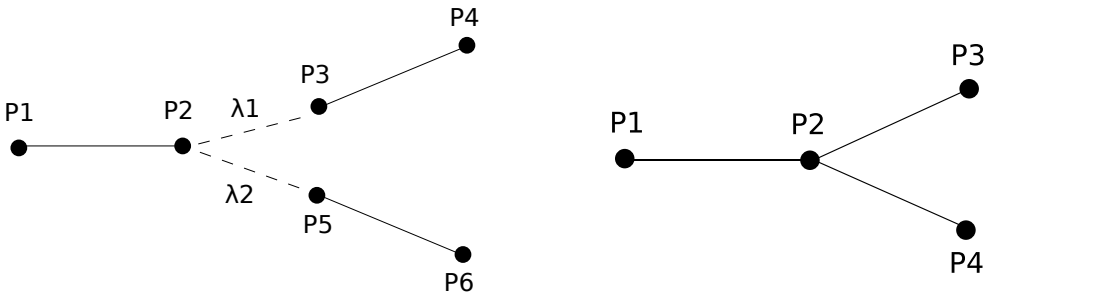

(a) STM bifurcation where static pressure is satisfied at junction interface.

(b) ETM bifurcation where λ_1 and λ_2 are Lagrange multipliers holding the total pressure as a constraint.

Figure 1. Difference in treatment of junctions of STM and ETM schemes.

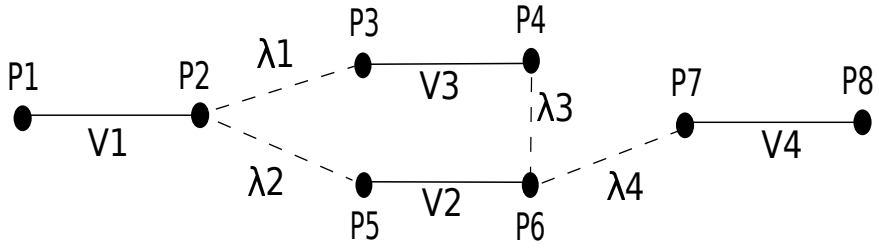

Figure 2. Configuration for bifurcation and unification test

The ETM scheme requires the system equations to be in the same form as equation (21). As a result, the junction constraints (including both pressure and flow) need to follow the same format. Linearisations for the conservation of total pressure terms are as follows

$$P^{n+1} \approx P^{n+1,k+1}, \quad \frac{\rho}{2}\left(\frac{Q^2}{A^2}\right)^{n+1} \approx \frac{\rho}{2}\left(\frac{Q^2}{A^2}\right)^{n+1,k}, \tag{40}$$

where k is the iteration level. As mentioned before only one solve is performed per time step (no iterations), hence, the iteration levels $(n+1,k) \approx (n)$ and $(n+1,k+1) \approx (n+1)$. Only the conservation of total pressure is needed as a constraint during the pressure solver, i.e. per bifurcation only two constraints are required. These are given by constraint (29) with $N = 2$ for a bifurcation, and represented by λ_1 and λ_2 in Figure 1b. The conservation of mass will be shown to be automatically satisfied in Section 3.3. Note that static pressure can also be used if desired by simply removing the dynamic pressure term $\frac{\rho}{2}\frac{Q^2}{A^2}$.

3.3 Physical Interpretation of The Lagrange Multipliers

In order to determine a physical interpretation of the Lagrange multipliers it is advantageous to consider one parent vessel connecting to one daughter vessel, which can then be easily extended to multiple parent or daughter vessels. Consider the last element in the parent vessel p_1 and the first element in its daughter vessel d_1. The system of equations representing this system is given by

$$\begin{bmatrix} ke_{11}^{p_1} & ke_{12}^{p_1} & 0 & 0 \\ ke_{21}^{p_1} & ke_{22}^{p_1} & 0 & 0 \\ 0 & 0 & ke_{11}^{d_1} & ke_{12}^{d_1} \\ 0 & 0 & ke_{21}^{d_1} & ke_{22}^{d_1} \end{bmatrix} \begin{bmatrix} P_1^{p_1} \\ P_2^{p_1} \\ P_1^{d_1} \\ P_2^{d_1} \end{bmatrix}^{n+1} = \begin{bmatrix} f_1^{p_1} \\ f_2^{p_1} \\ f_1^{d_1} \\ f_2^{d_1} \end{bmatrix}^{n} + \begin{bmatrix} Q_1^{p_1} \\ -Q_2^{p_1} \\ Q_1^{d_1} \\ -Q_2^{d_1} \end{bmatrix}^{n+1} . \tag{41}$$

Noting that the final column on the right hand side of Equation (41) represents the flow rate column. The first flow of the system $Q_1^{p_1}$ and the last flow of the system $Q_2^{d_1}$ will either: become the conservation of mass when connected another element within the vessel as shown in Equation (23) (becomes zero); or be a specified boundary condition, which could be either prescribed flow or pressure. After taking this into account the only flows left in this column are the outflow of the parent vessel $Q_2^{p_1}$, and, the inflow of the daughter vessel $Q_1^{d_1}$. However, from mass conservation the outflow of the parent vessel must equal the inflow of the daughter vessel. Defining $\lambda_1 = Q_2^{p_1} = Q_1^{d_1}$ and adding it as a variable to the left hand side of system (41), and adding the conservation of total pressure equation (29) between one parent vessel and one daughter vessel gives

$$\begin{bmatrix} ke_{11}^{p_1} & ke_{12}^{p_1} & 0 & 0 & 0 \\ ke_{21}^{p_1} & ke_{22}^{p_1} & 0 & 0 & 1 \\ 0 & 0 & ke_{11}^{d_1} & ke_{12}^{d_1} & -1 \\ 0 & 0 & ke_{21}^{d_1} & ke_{22}^{d_1} & 0 \\ 0 & 1 & -1 & 0 & 0 \end{bmatrix} \begin{bmatrix} P_1^{p_1} \\ P_2^{p_1} \\ P_1^{d_1} \\ P_2^{d_1} \\ \lambda_1 \end{bmatrix}^{n+1} = \begin{bmatrix} f_1^{p_1} \\ f_2^{p_1} \\ f_1^{d_1} \\ f_2^{d_1} \\ f_{\lambda_1} \end{bmatrix}^{n} . \tag{42}$$

This implies that the Lagrange multiplier is in fact the flow between parent vessel and daughter vessel. Writing the equations corresponding to the last node of the parent and the first node of the daughter gives

$$ke_{21}^{p_1} P_1^{p_1} + ke_{22}^{p_1} P_2^{p_1} + \lambda_1 = f_2^{p_1}, \tag{43}$$

$$ke_{11}^{d_1} P_1^{d_1} + ke_{12}^{d_1} P_2^{d_1} - \lambda_1 = f_2^{d_1}. \tag{44}$$

Property	Units	Vessel 1	Vessel 2	Vessel 3	Vessel 4
Length, L	cm	400	400	400	400
Radius, r_d	cm	1.3	0.8	1.1	1.3
Area, A_d	cm^2	5.3093	2.3093	3.8013	5.3093
Initial area, $A(x,0)$	cm^2	5.3093	2.3093	3.8013	5.3093
Initial flow, $Q(x,0)$	$\text{cm}^2\,\text{s}^{-1}$	0	0	0	0
Initial pressure, $P(x,0)$	kPa	10.666	10.666	10.666	10.666
Wall thickness, h	cm	0.07	0.07	0.07	0.07
Blood density, ρ	$\text{kg}\,\text{m}^{-3}$	1060	1060	1060	1060
Blood viscosity, μ	mPa s	4	4	4	4
Velocity profile order ζ	—	9	9	9	9
Young's modulus, E	kPa	700.0	700.0	700.0	700.0
Diastolic pressure, P_d	kPa	10.666	10.666	10.666	10.666
External pressure, P_{ext}	Pa	0	0	0	0
Outflow pressure, P_{out}	Pa	0	0	0	0
Windkessel resistance, R_1	$\text{Pa}\,\text{s}\,\text{m}^{-3}$	—	—	—	∞
Daughter Vessel(s),	—	Vessel 2& 3	Vessel 4	Vessel 4	—
Parent Vessel(s),	—	—	Vessel 1	Vessel 1	Vessel 2& 3

Table I. Properties for Bifurcation to Unification Test

A dimensional analysis can be done on either of these equations to find that λ_1 has the same units of flow rate.

This can be extended to any number of parent vessels and any number of daughter vessels. For example, at a bifurcation, the equations of the last node of the parent vessel and the first node of the two daughter vessels are

$$ke_{21}^{p_1}P_1^{p_1} + ke_{22}^{p_1}P_2^{p_1} + \lambda_1 + \lambda_2 = f_2^{p_1}, \tag{45}$$

$$ke_{11}^{d_1}P_1^{d_1} + ke_{12}^{d_1}P_2^{d_1} - \lambda_1 = f_2^{d_1}, \tag{46}$$

$$ke_{11}^{d_2}P_1^{d_2} + ke_{12}^{d_2}P_2^{d_2} - \lambda_2 = f_2^{d_2}. \tag{47}$$

It is easily seen that λ_1 is the inlet flow of the first daughter vessel and λ_2 is the inlet flow of the second daughter vessel and hence $\lambda_1 + \lambda_2$ is the total flow leaving (or entering) the parent vessel.

In the case of two parent vessels to one daughter vessel the equations of the last node of the two parents and first node of the daughter become

$$ke_{21}^{p_1}P_1^{p_1} + ke_{22}^{p_1}P_2^{p_1} + \lambda_1 + \lambda_2 = f_2^{p_1}, \tag{48}$$

$$ke_{21}^{p_2}P_1^{p_2} + ke_{22}^{p_2}P_2^{p_2} - \lambda_1 = f_2^{p_2}, \tag{49}$$

$$ke_{11}^{d_1}P_1^{d_1} + ke_{12}^{d_1}P_2^{d_1} - \lambda_2 = f_2^{d_1}. \tag{50}$$

The Lagrange multiplier $\lambda_1 = -Q_2^{p_2}$ (negative the outlet flow of the second parent vessel), while λ_2 is the inlet flow of the daughter vessel, hence, $\lambda_1 + \lambda_2$ will be the outlet flow of the first parent (reference) vessel. This can be extended to any number of parent and/or daughter vessels.

Thus the use of Lagrange multipliers to constrain conservation of total pressure (static pressure can also easily be used) also finds the external flows of the vessels, meaning that conservation of mass is also automatically satisfied for the connected vessels.

Property	Units	Vessel 1
Length, L	cm	3780
Area, A_d	cm^2	5.6549
Initial flow, $Q(x,0)$	$\mathrm{cm}^2\,\mathrm{s}^{-1}$	0
Wall thickness, h	cm	0.3
Blood density, ρ	$\mathrm{kg\,m}^{-3}$	1060
Blood viscosity, μ	mPa s	0
Velocity profile order ζ	—	9
Young's modulus, E	kPa	700.0
Diastolic pressure, P_d	kPa	10.9333
External pressure, P_{ext}	Pa	0
Inflow pressure, P_{In}	kPa	16.3995
Outflow pressure, P_{out}	Pa	10.9333

Table II. Properties for shock wave Test

4 Results

It should be noted that in this section only those results are shown where constraints were imposed using Lagrange multipliers. The same simulations have been performed using the penalty method and results of both methods are almost indistinguishable. However, Lagrange multipliers are shown to be external pressure, meaning mass is conserved at junctions when imposing total pressure as a constraint, which is not the case with the penalty method. In Section 4.1 a small configuration of a vessel bifurcation to a re-unification is performed, while a shock example is shown in 4.2. In Sections 4.3, 4.4, 4.5, 4.6, 4.7 and 4.8 the results for the benchmark problems on the single pulse in a vessel, common carotid, upper thoracic aorta, aortic bifurcation, 37-segment arterial tree and 56-segment arterial tree are presented and compared to the results of the LCG method in [31] (the other schemes presented in [31] gave consistent results with the LCG method). All simulations were performed in MATLAB Student R2013a (The MathWorks, Inc., Natick, MA, USA) on an Intel Core i5-3337U 1.8GHz with turbo boost up to 2.7GHz. It should be noted that for tests containing a single vessel the ETM scheme and STM scheme will be identical as the only difference is the treatment at vessel junctions.

4.1 Single Pulse In Bifurcation And Unification

In this test there are four vessels with properties given in Table I and the problem configuration shown in Figure 2. The exact solution is not known for this problem. This test is used to confirm the physical interpretation of the Lagrange multipliers for two main types of vessel junctions, a bifurcation (one parent vessel connected to two daughter vessels) and a unification (two parent vessels connected to one daughter vessel). The time step is $\Delta t = 1\,\mathrm{ms}$ and element size is $\Delta x =$

1 cm. The boundary condition at the inlet is

$$Q_{inlet} = \begin{cases} 40\sin(\frac{\pi t}{0.3636T}), & \text{for} \quad 0 < t \leq 0.3636T, \\ \\ 0, & \text{for} \quad 0.3636T < t \leq T, \end{cases} \tag{51}$$

with cardiac period $T = 1.1$ s. The outlet boundary condition (outlet of vessel 4) is a resistance set at infinity and the simulation is run for 4 cardiac cycles, which allows the network to experience both positive and negative flow rates at all the junctions. Figure 3 shows the flow rate waveforms at the junctions, which are compared with values of the Lagrange multipliers at each junction. At the bifurcation shown in Figure 3a the values for the outlet flow of the parent (vessel 1) are equal to the sum of Lagrange multipliers λ_1 and λ_2 as discussed in Section 3.3, and the inlet flow rates of the two daughter vessels (vessels 2,3) are equal to the values of λ_1 and λ_2 respectively. At the unification of vessels 2 and 3 connecting to vessel 4, The reference parent vessel (vessel 2) is equal to the sum of Lagrange multipliers λ_3 and λ_4, while the other parent vessel (vessel 3) has in outlet flow rate equal to the negative of λ_3, and the daughter vessel (vessel 4) inlet flow is equal to λ_4.

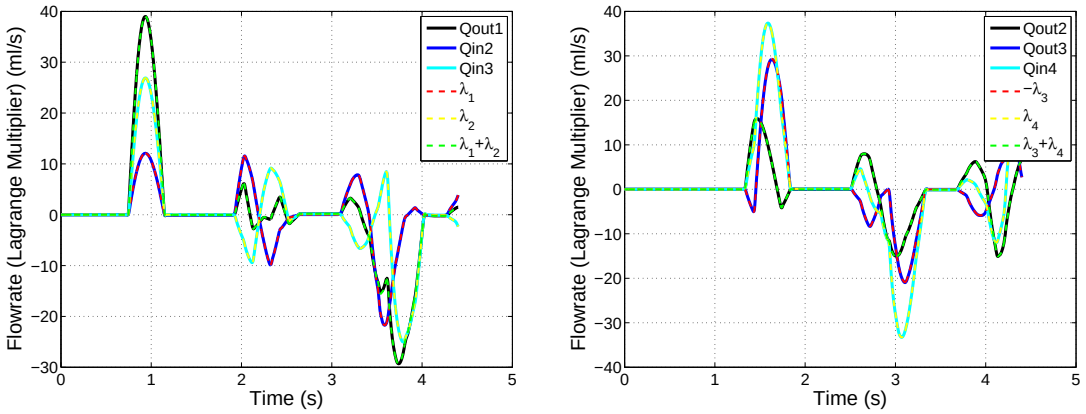

(a) Junction 1 (Bifurcation)

(b) Junction 2 (Unification)

Figure 3. A comparison Of Outflow/Inflow at Junctions with Lagrange Multipliers

4.2 Shockwave within a vessel

The vessel properties and parameters of the shock example are given in Table II. In this example the fluid is considered inviscid ($\mu = 0$), while boundary conditions at both inlet and outlet are reflection free. The time step is $\Delta t = 0.5$ ms and element size is $\Delta x = 1$ cm. The initial pressure is discontinuous and is given by

$$P_{initial}(x) = \begin{cases} 16.3995\,\text{kPa} & \text{if} \quad x < \frac{L}{2}, \\ \\ 10.9333\,\text{kPa} & \text{if} \quad x \geq \frac{L}{2}. \end{cases} \tag{52}$$

Figure 4 shows results for the ETM scheme compared with an analytical solution (see [35] for details of the analytic solution). The flow rate and pressure waveforms as shown in Figures 4a and 4c

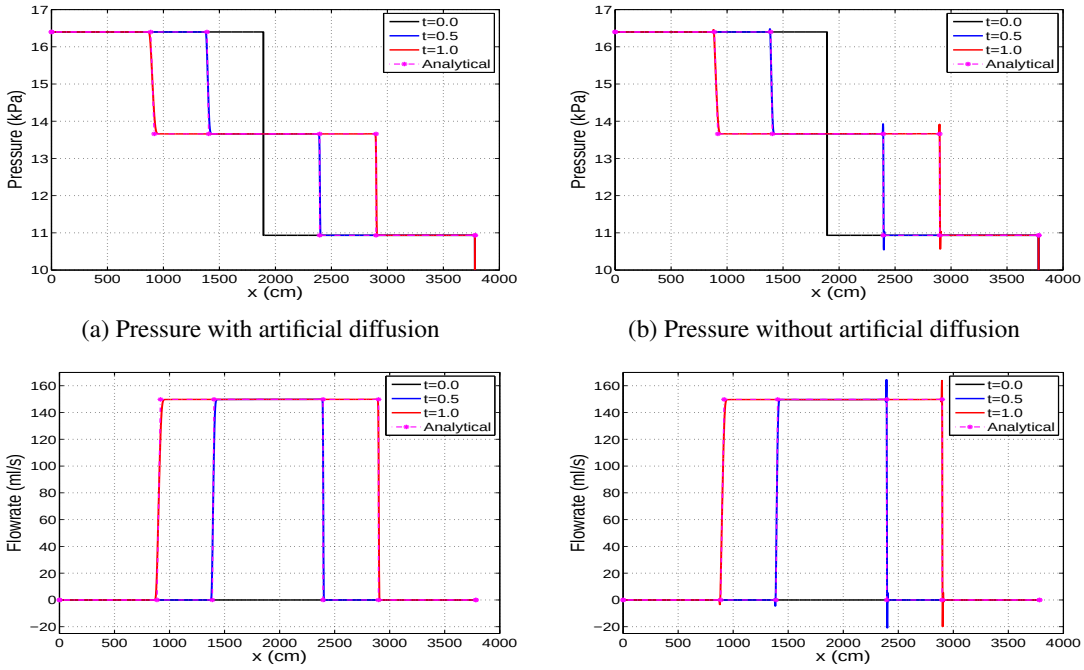

(a) Pressure with artificial diffusion

(b) Pressure without artificial diffusion

(c) Flow Rate with artificial diffusion

(d) Flow Rate without artificial diffusion

Figure 4. Pressure and flow rate waveforms for shock test with and without artificial diffusion at different time instances (seconds).

includes an artificial diffusion applied via a splitting technique that involves an extra computational step in the form

$$\frac{Q_j^{n+1}}{\Delta t} - \frac{200}{A_i^{n+1}} \frac{Q_{j+1}^{n+1} - 2Q_j^{n+1} + Q_{j-1}^{n+1}}{(\Delta x)^2} = \frac{\bar{Q}^{n+1}}{\Delta t}, \tag{53}$$

where $\bar{Q}^{n+1}$ is the flow rate solution from solving system (19). Without this artificial diffusion the solution develops oscillations as shown in Figures 4b and 4d. This artificial diffusion was applied over the entire vessel (not just in the region of the shock). The results indicate that the ETM correctly predicts the position of the right travelling shock and the left travelling rarefaction.

4.3 Single Pulse In a Reflection Free Vessel

A vessel with uniform properties is used with a reflection-free outflow boundary condition. At the inlet the inflow is a Gaussian-shaped wave. A theoretical solution using a linearised system is used and is suitable for small fluid velocity. For more details on this test see [31] and [36] for the theoretical solution. The time step for the ETM scheme is $\Delta t = 0.1\,\text{ms}$ and element size is $\Delta x = 0.1\,\text{cm}$. Two different variations are considered, with a viscous case and an inviscid case. Figure 5a shows the ETM method for both the viscous and inviscid case. The theoretical decrease of the peak for the viscous case is the black line. In the inviscid case the peak pressure for the ETM method has very good agreement with theoretical peak pressure, and, has very good agreement with the expected peak decrease for the viscous case.

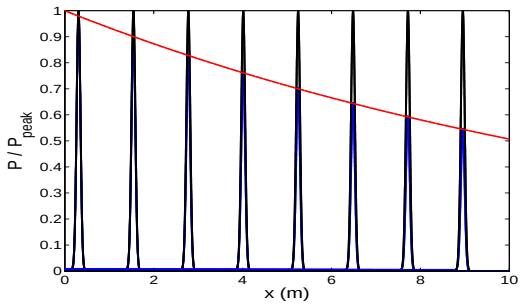

(a) Single Pulse ETM scheme. Pressure of inviscid case (black line). Pressure of viscous case (blue line). Theoretical decrease of pressure for viscous case (red line)

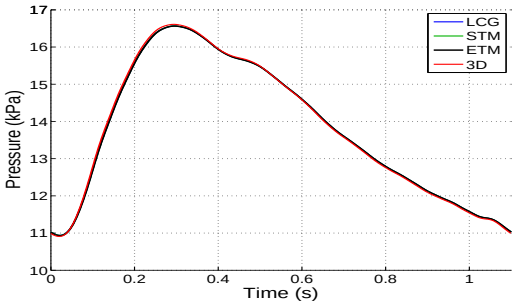

(b) Pressure in common carotid artery test

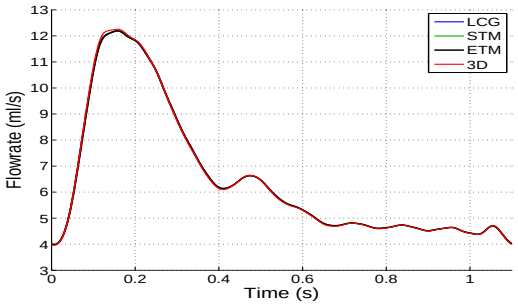

(c) Flow rate in common carotid artery test

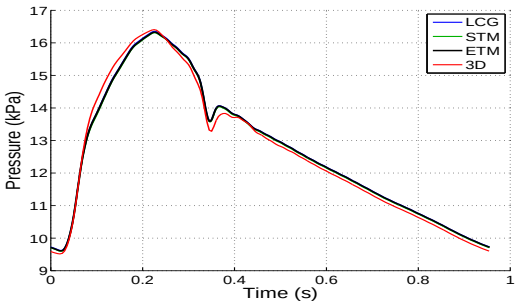

(d) Pressure in upper thoracic aorta test

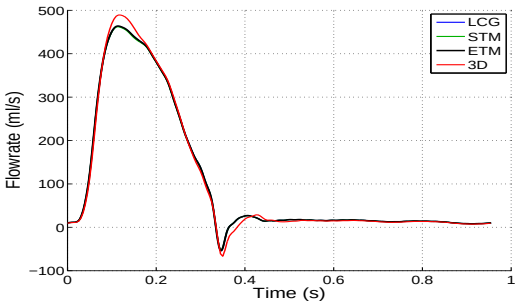

(e) Flow rate in upper thoracic aorta test

Figure 5. Pressure in Single Pulse test for ETM, Common Carotid Artery test comparing pressure and flow rate waveforms in ETM, STM, LCG and 3D data, Upper thoracic Aorta test comparing pressure and flow rate waveforms in ETM, STM, LCG and 3D data

4.4 Common Carotid Artery

The common carotid artery model considered has uniform properties and is modelled as a single vessel. The end of the vessel is connected to a three element Windkessel model, for details on this test see [31] and [37]. For the ETM scheme the time step used is $\Delta t = 1\,\text{ms}$ and element size is $\Delta x = 1\,\text{cm}$. Figures 5b and 5c show that both pressure and flow rate waveforms show good agreement with the 3D data for all methods shown.

The convergence plot in Figure 6 shows the convergence rate of the flow. The ETM scheme is first simulated with an element size of $\Delta x = 0.05\,\text{cm}$ and time step of $\Delta t = 0.05\,\text{ms}$, which is used as a reference solution. Then the ETM is simulated for different Δx with Δt kept constant at

$\Delta t = 0.05$ ms, and different Δt with Δx kept constant at $\Delta x = 0.05$ cm. The error is determined at the middle of the vessel. The method shows super-linear convergence in both time and space.

4.5 Upper Thoracic Aorta

The thoracic aorta is considered to be a single vessel with uniform properties coupled with a three element Windkessel to simulate the effect of the rest of the systemic circulation [37]. See [31] for more details on the test. Figures 5d and 5e show the pressure and flow waveforms for the ETM, STM and LCG, along with a 3D solution. All three 1D methods are in agreement with each other with some differences with the 3D data, particularly during systole. The time step used for the ETM scheme is $\Delta t = 1$ ms and element size is $\Delta x = 1$ cm.

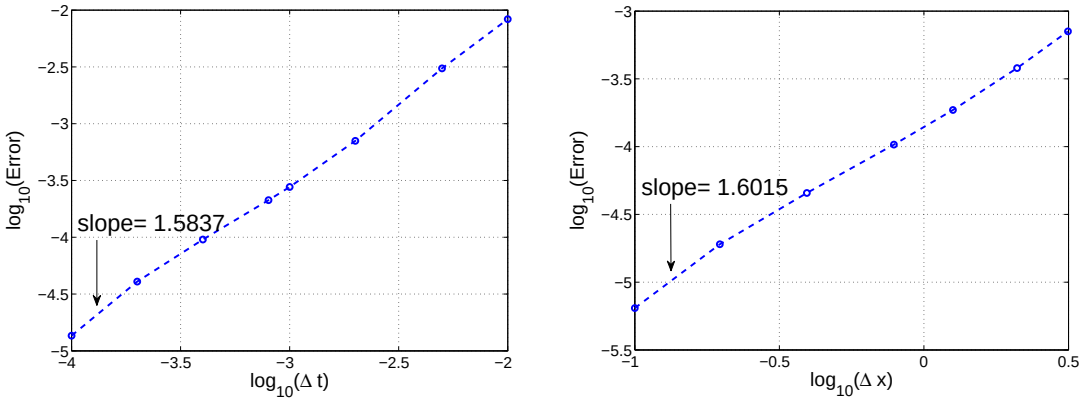

(a) Convergence curve for different timesteps

(b) Convergence curve for different element sizes

Figure 6. Convergence Curves for ETM in the common carotid artery test for flow rates. The Error taken at the centre at the vessel, with a reference solution using $\Delta x = 0.05$ cm and $\Delta t = 0.05$ ms

4.6 Aortic Bifurcation

The aortic bifurcation problem consists of an abdominal aorta connected to two iliac arteries. The bifurcation model is symmetric, i.e. both iliac arteries are identical and the vessels considered have uniform properties. See [31] and [37] for more details. For the ETM scheme the time step used is $\Delta t = 1$ ms and element size is $\Delta x = 1$ cm. Figure 7 shows the STM, ETM and LCG methods compared with the 3D data. Both pressure and flow waveforms show good agreement with the 3D data in both the abdominal aorta and common iliac arteries.

4.7 Thirty Seven Arterial Tree Network

The arterial tree simulated was presented in [38], with *in vitro* flow and pressure measurements. The tree comprises of the largest central systemic arteries. The model uses *in vitro* flow rate measurements as an inlet boundary condition, while the outflow boundaries are attached to resistance elements (see [31] for details on parameters). Figure 8 shows the results for the aortic arch II and the iliac-femoral II arteries for both pressure and flow rate. The methods compared are the ETM, STM and LCG, along with in vitro data provided in [31].

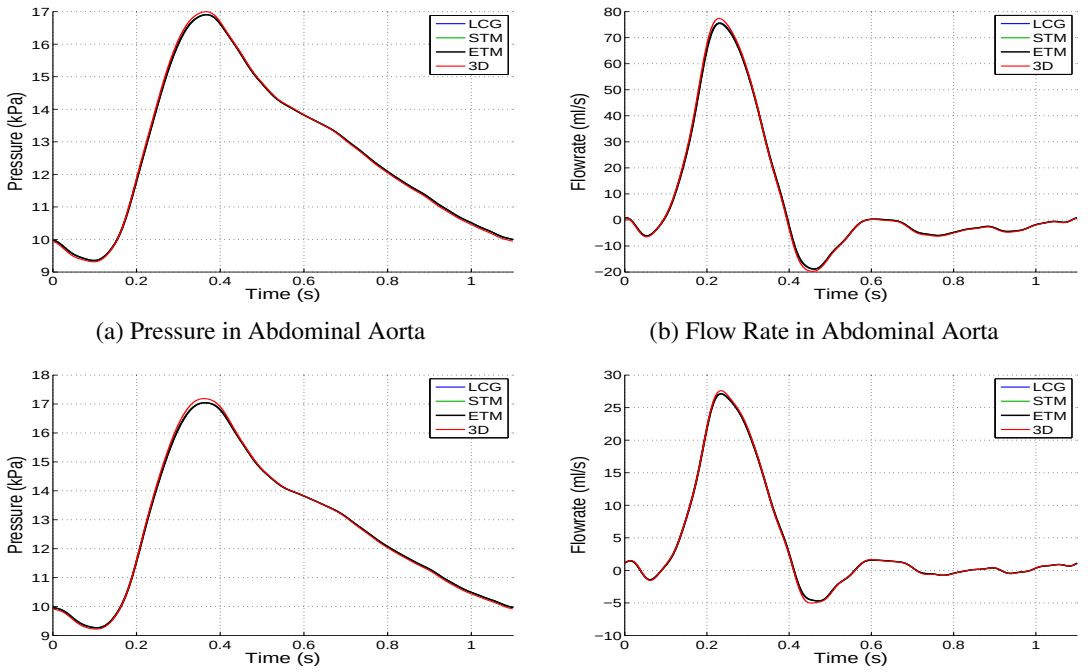

(a) Pressure in Abdominal Aorta

(b) Flow Rate in Abdominal Aorta

(c) Pressure in Iliac Arteries

(d) Flow Rate in Iliac Arteries

Figure 7. Aortic Bifurcation. Pressure and flow rate comparison of ETM, STM and LCG schemes with 3D data [31]

For the ETM scheme the time step used is $\Delta t = 1\,\text{ms}$ and the element size used is $\Delta x = 1\,\text{cm}$. The maximum CFL for this problem is $CFL = 2.3517$ and the simulation takes an average of 2.2 seconds per cardiac cycle. The results are consistent with the numerical schemes. When compared to the *in vitro* measurements, the numerical results over predict the high frequency oscillations in both pressure and flow for the second and third vessel generations.

4.8 The ADAN56 Arterial Tree

The ADAN56 model is a reduced version of an arterial network which was developed in Blanco *et al.* [15],[16]. The arterial tree consists of 56 arteries. For details on parameters and arterial tree data see [31]. The results for the ADAN56 case show that the ETM scheme improves the solution significantly when compared with the original STM. Figure 9 shows the solution of both pressure and flow waveforms in the right internal carotid artery, right anterior tibial and right renal, respectively. The time step used for the ETMa scheme is $\Delta t = 1\,\text{ms}$ and the element size used is $\Delta x = 1\,\text{cm}$, while in ETMb $\Delta t = 2\,\text{ms}$ and $\Delta x = 2\,\text{cm}$, and in ETMc $\Delta t = 5\,\text{ms}$ and $\Delta x = 5\,\text{cm}$. The ETM scheme shows good agreement with results of the schemes in [31], with only small discrepancies for larger times steps ($\Delta t = 2\,\text{ms}$ and $\Delta t = 5\,\text{ms}$). Table III shows the run time and maximum CFL number for each ETM simulation.

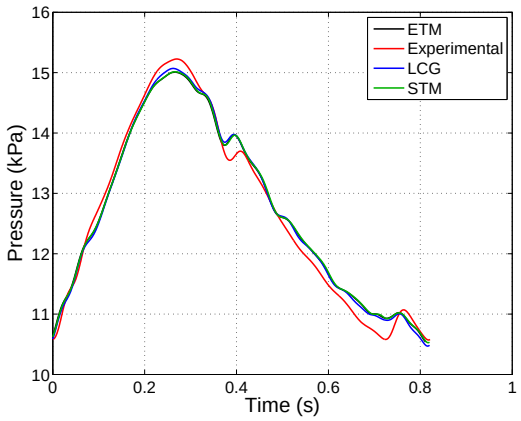

(a) Pressure Error in Aortic Arch II

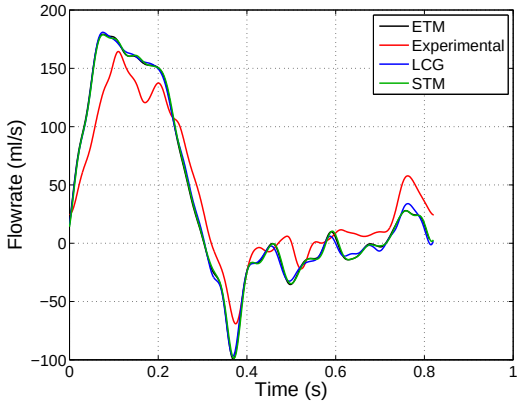

(b) Flow Rate Error in Aorta Arch II

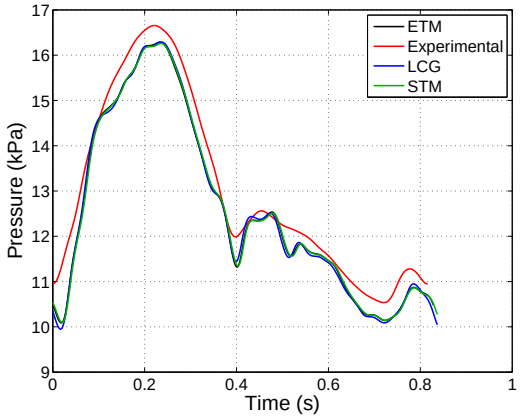

(c) Pressure Error in Iliac-Femoral II

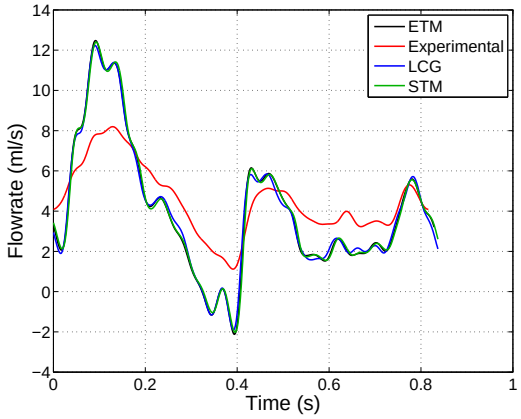

(d) Flow Rate Error in Iliac-Femoral II

Figure 8. 37-Artery Tree. Pressure and flow waveforms in Aortic Arch II and Iliac-Femoral II, comparison between ETM,STM,LCG and experimental

5 Discussion

The ETM scheme was developed by extending the already existing STM scheme as proposed in [33]. This modification involves the use of Lagrange multipliers at vessel junctions to constrain conservation of total pressure (static pressure can also easily be used). The Lagrange multipliers were shown to represent external flow rates of vessels, and hence conservation of mass is automatically satisfied. The ETM scheme is stable for any CFL number, which allows for a number of cardiac cycles to be performed using larger element sizes and time steps to determine a good initial guess, before using a refined spatial and temporal mesh for 1-2 cardiac cycles to converge to the periodic solution.

ETM Run	Time Step (ms)	Max Element Size (cm)	Max CFL	Time
a	1	1	3.0332	4.44
b	2	2	6.0668	1.48
c	5	5	15.1605	0.39

Table III. ETM scheme for different time steps and element sizes

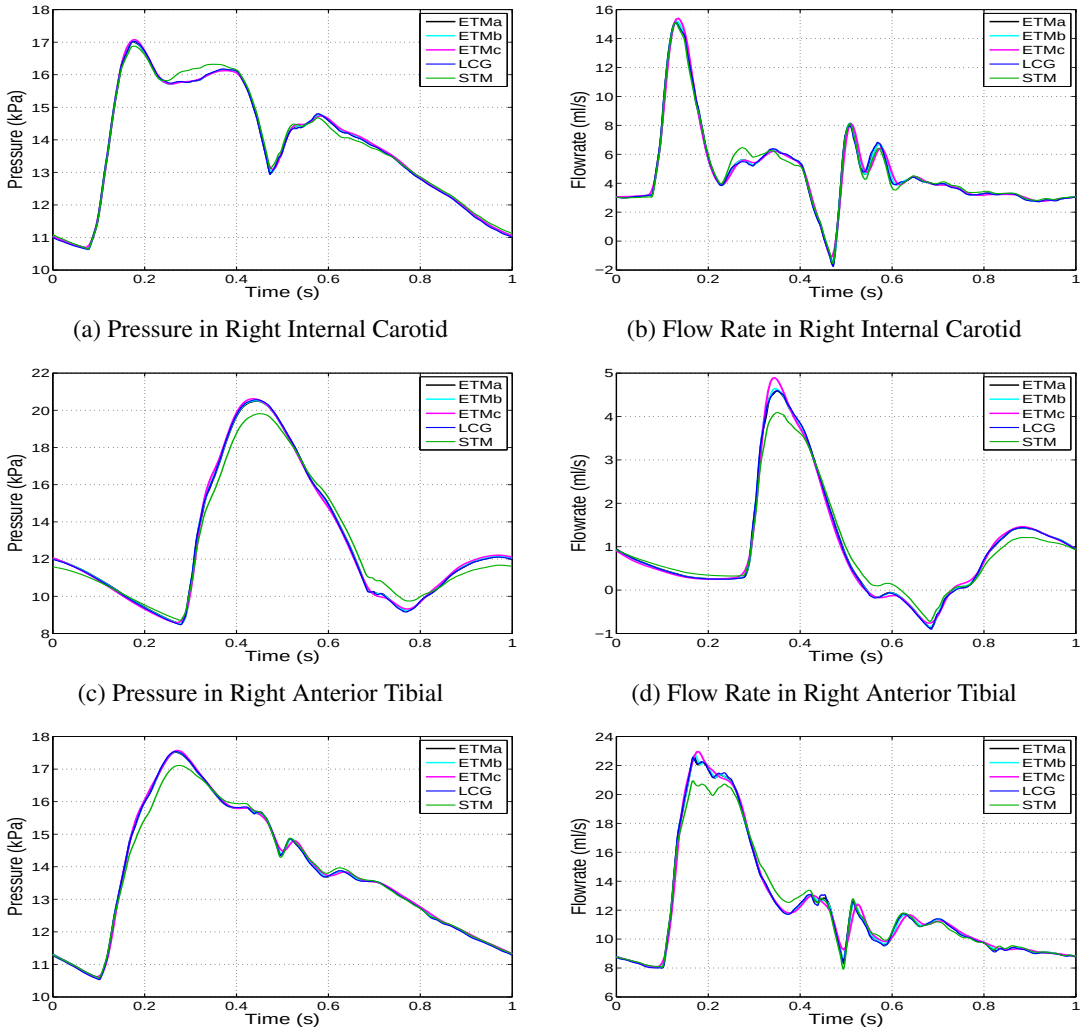

(a) Pressure in Right Internal Carotid

(b) Flow Rate in Right Internal Carotid

(c) Pressure in Right Anterior Tibial

(d) Flow Rate in Right Anterior Tibial

(e) Pressure in Right Renal

(f) Flow Rate in Right Renal

Figure 9. Pressure and flow rate waveforms in right internal carotid and right anterior tibial, comparing ETM, STM and LCG methods. ETMa is the ETM scheme with $\Delta t = 1$ ms and $\Delta x = 1$ cm, ETMb is the ETM scheme with $\Delta t = 2$ ms and $\Delta x = 2$ cm, ETMc is the ETM scheme with $\Delta t = 5$ ms and $\Delta x = 5$ cm.

The ETM scheme was first applied to a small network configuration involving a bifurcation, a unification, and a reflective boundary condition. This means that both forward and backward flows occurred at vessel junctions. Moreover, the test confirmed that the Lagrange multipliers corresponded to external flows, meaning that conservation of mass is also being satisfied, whilst only using the conservation of total pressure to constrain the system.

A shock example was implemented with the initial conditions of zero flow and a discontinuous pressure (similar to a dam break in the 1D Saint Venant equations). The ETM was compared with an analytical solution and was shown to contain oscillations with no special treatment. However, these oscillations were shown to be eliminated by simply adding a small amount of artificial diffusion. The method was also able to correctly predict the positions of the shock and rarefaction. Although a more thorough investigation is needed for the ETM scheme with regards to shocks, it is outside the scope of this current work.

The single pulse model propagates a narrow Gaussian shaped wave in a vessel with a reflection-free outlet boundary condition. A theoretical solution exists for both the inviscid and viscid cases. The wave has a very small wavelength when compared with the length of the vessel. As mentioned in [31], very high frequencies will dominate which is numerically more challenging. The results show that the ETM scheme gives good agreement with the theoretical solution and therefore can capture high frequencies.

Two single vessel cases and an aortic bifurcation were considered under physiological conditions. These cases have 3D solutions available from [37]. The results of the ETM (identical to STM in the single vessel cases) give excellent agreement with the other schemes presented in [31] and capture the main features of the 3D data.

The 37 vessel arterial tree presented in [38] is made up of 37 silicone vessels to represent the main arteries in the human systemic system. *In vitro* pressure and flow rate measurements were taken at multiple locations. At the inlet of the model the measured *in vitro* flow rate is prescribed. The ETM scheme was shown to give results consistent with all other numerical schemes presented in [31]. Though there were discrepancies between experimental and numerical results.

The ADAN56 arterial system includes the largest 56 arteries in the human systemic system. The anatomy and mechanical properties of vessels and inflow and outflow boundary conditions are based all human physiological data. The ETM was shown to improve upon the solution of the STM method. Thus, confirming the conclusion in [31] that the discrepancies for the solution of the STM were due to the method imposing conservation of static pressure at vessel junctions. The results of the ETM scheme show good agreement with the LCG method [9], which is consistent with the other methods presented in [31].

6 Conclusions

The aim of this paper was to investigate the use of an implicit solver for the 1D blood flow equations, and the possible use of Lagrange multipliers and penalty methods to constrain vessel junctions using dynamic pressure and mass conservation. This led to the newly developed ETM, which extends the STM method by using Lagrange multipliers to constrain conservation of total pressure at vessel junctions. The Lagrange multipliers were shown to physically represent the flow at the outlets (or inlets) of vessels, ensuring mass conservation and allowing both forward and backward flow rates at vessel junctions without the need to use characteristics and Newton-Raphson iterations, which are needed for explicit methods. If shocks or high gradients are present, the ETM scheme needs artificial diffusion in order to capture the shock and rarefaction without spurious oscillations. The ETM scheme was shown to give results in agreement with the methods presented in [31], for all benchmark tests. The ETM method improved the solution of both pressure and flow rate waveforms significantly in the ADAN56 network when compared with the original STM, and has shown excellent agreement with other published schemes in [31]. The implicit nature of the ETM scheme means no restrictive stability criterion such as the CFL condition is needed. The scheme works in a similar way to a split method, with pressures and Lagrange multipliers solved for implicitly once per time step. The flow rates are then updated at the element level from the updated pressures. Limitations of the model are similar to the STM method [33], where the coupling equations need to be in the same form as the fluid flow equations. The model also requires each element to have only

two nodes and hence, higher order spatial approximations are not possible. Overall the results of the ETM have showed excellent agreement with other commonly used methods presented in [31]. The implementation of boundary conditions and ease of connecting the 1D blood flow model with any 0D Windkessel models are also a strength of the method.

References

[1] HUGHES JR, LUBLINER J. *On the One-Dimensional Theory of Blood Flow in the Larger Vessels. Mathematical Biosciences, 1973;* ***18****: 161-170.*

[2] STERGIOPOULOS N. *Computer simulation of arterial blood flow. 1990; Retrospective Theses and Dissertations. Paper 9896. Iowa State University.*

[3] STERGIOPOULOS N, YOUNG D, ROGGE T. *Computer simulation of arterial blood flow with applications to arterial and aortic stenoses. Journal Of Biomechanics, 1992;* ***25****: 1477-1488.*

[4] OLUFSEN M, PESKIN C, KIM W, PEDERSEN E, NADIM A, LARSEN J. *Numerical simulation and experimental validation of blood flow in arteries with structured-tree outflow conditions. Annals of Biomedical Engineering 2000;* ***28****: 12811299.*

[5] FORMAGGIA L, LAMPONI D, QUARTERONI A. *One-dimensional models for blood flow in arteries. Journal of Engineering Mathematics, 2003;* ***47****: 251-276.*

[6] HELLEVIK LR, VIERENDEELS J, KISERUD T, STERGIOPULOS N, IRGENS F, DICK E. *An assessment of ductus venosus tapering and wave transmission from the fetal heart. Biomechanics and Modeling in Mechanobiology 2009;* ***8****(6):509517.*

[7] BESSEMS D, RUTTEN M, VAN DE VOSSE F. *A wave propagation model of blood flow in large vessels using an approximate velocity profile function. Journal Of Fluid Mechanics, 2007;* ***580*** *: 145-168. DOI: 10.1017/S0022112007005344.*

[8] SHERWIN SJ, FORMAGGIA L, PEIRÓ J, FRANKE V. *Computational modelling of 1d blood flow with variable mechanical properties and its application to the simulation of wave propagation in the human arterial system. International Journal For Numerical Methods In Fluids, 2003;* ***43****: Issue 6-7 : 673-700.*

[9] MYNARD JP, NITHIARASU P. *A 1D arterial blood flow model incorporating ventricular pressure, aortic valve and regional coronary flow using the locally conservative Galerkin (LCG) method. Communications In Numerical Methods In Engineering, 2008;* ***24*** *: 367-417.*

[10] MÜLLER LO, TORO EF. *Well-balanced high-order solver for blood flow in networks of vessels with variable properties. International Journal For Numerical Methods In Biomedical Engineering, 2013;* ***29*** *: 1388-1411.*

[11] MÜLLER LO, TORO EF. *A global multiscale mathematical model for human circulation with emphasis on the venous system. International Journal For Numerical Methods In Biomedical Engineering, 2014;* ***30*** *: 681-725.*

[12] MÜLLER LO, TORO EF. *Enhanced global mathematical model for studying cerebral venous blood flow. Journal of Biomechanics, 2014;* ***47*** *: 3361-3372.*

[13] LOW K, VAN LOON R, SAZONOV I, BEVAN RLT, NITHIARAASU P. *An improved baseline model for a human arterial network to study the impact of aneurysms on pressure-flow waveforms. International Journal For Numerical Methods In Biomedical Engineering, 2012;* ***28*** *: 1224-1246.*

[14] BLANCO PJ, FEIJÓO RA, URQUIZA SA. *A unified variational approach for coupling 3D-1D models and its blood flow applications. Computer methods in applied mechanics and engineering, 2007;* ***196*** *: 4391-4410.*

[15] BLANCO PJ, WATANABE S, DARI E, PASSOS M, FEIJÓO RA. *Blood flow distribution in an anatomically detailed arterial network model:criteria and algorithms. Biomechanics and Modelling in Mechanobiology 2014;* ***13*** *: 1303-1330.*

[16] BLANCO PJ, WATANABE S, PASSOS M, LEMOS P, FEIJÓO RA. *An anatomically detailed arterial network model for one-dimensional computational hemodynamics. IEEE Transactions on Biomedical Engineering 2015;* ***62*** *: 736-753.*

[17] MALOSSI ACI, BLANCO PJ, CROSETTO P, DEPARIS S, QUARTERONI A. *Implicit Coupling of One-Dimensional And Three-Dimensional Blood Flow Models With Compliant Vessels. Society for Industrial and Applied Mathematics, 2013;* ***11*** *; No. 2: 474-506.*

[18] BLANCO PJ, FEIJÓO RA. *An dimensionally-heterogeneous closed-loop model for the cardiovascular system and its applications. Medical Engineering % Physics 2013;* ***35*** *: 652-667.*

[19] FORMAGGIA L, GERBEAU JF, NOBILE F, QUARTERONI. *On the Coupling of 3D and 1D Navier-Stokes Equations for Flow Problems in Compliant Vessels. Computer Methods in Applied Mechanics and Engineering 2001; Vol* ***191*** *: Issue 6-7: pages 561-582. doi:10.1016/S0045-7825(01)00302-4.*

[20] CASULLI V, DUMBSER M, TORO, EF *Semi-implicit numerical modeling of axially symmetric flows in compliant arterial systems International Journal For Numerical Methods In Biomedical Engineering, 2012,* ***28*** *: 257-272. DOI: 10.1002/cnm.1464.*

[21] WATANABE SM, BLANCO PJ, FEIJÓO RA. *Mathematical Model of Blood Flow in an Anatomically Detailed Arterial Network of The Arm. ESAIM: Mathematical Modelling and Numerical Analysis 2013.* ***47****: 961-985.*

[22] KEIJSERS JMT, LEGUY CAD, HUBERTS W, NARRACOTT AJ, RITTWEGER J, VAN DE VOSSE FN. *A 1D pulse wave propagation model of the hemodynamics of calf muscle pump function. International Journal For Numerical Methods In Biomedical Engineering, 2015; e02714.*

[23] URQUIZA SA, BLANCO PJ, VNERE MJ, FEIJÓO RA. *Multidimensional modelling for the carotid artery blood flow. Computer methods in applied mechanics and engineering, 2006;* ***195****: Issue 33-36 : 4002-4017.*

[24] ALASTRUEY J, MOORE SM, PARKER KH, DAVID T, PEIRÓ J, SHERWIN SJ. *Reduced modelling of blood flow in the cerebral circulation: Coupling 1-D, 0-D and cerebral autoregulation models. International Journal For Numerical Methods In Fluids, 2008;* ***56*** *: 1061-1067.*

[25] LEINAN P. *Biomechanical modeling of fetal veins: the umbilical vein and ductus venosus bifurcation. Ph.D. Thesis, Norwegian University of Science and Technology, NTNU, Trondheim, Norway.*

[26] MYNARD JP, DAVIDSON MR, PENNY DJ, SMOLICH JJ. *A numerical model of neonatal pulmonary atresia with intact ventricular septum and RV-dependant coronary flow. International Journal For Numerical Methods In Biomedical Engineering, 2010;* ***26*** *: 843-861.*

[27] MYNARD JP, DAVIDSON MR, PENNY DJ, SMOLICH JJ. *A simple, versatile valve model for use in lumped parameter and one-dimensional cardiovascular models. International Journal For Numerical Methods In Biomedical Engineering, 2011;* ***00*** *: 1-16.*

[28] MYNARD JP, SMOLICH JJ. *One-Dimensional Haemodynamic Modeling and Wave Dynamics in the Entire Adult Circulation. Annals of Biomedical Engineering, Vol 43, No 6, 1443-1460, 2015, DOI: 10.1007/s10439-015-1313-8.*

[29] ITU LM, SUCIU C, POSTELNICU A, MOLDOVEANU F. *Analysis of outflow boundary condition implementations for 1D blood flow models. Proceedings of the 3rd International Conference on E-Health and Bioengineering-EHB 2011, 24th-26th November, 2011; Iasi, Romania.*

[30] WANG X, FULLANA J-M, LAGRE P-Y. *Verification and comparison of four numerical schemes for a 1D viscoelastic blood flow model. Computer methods in Biomechanics and Biomedical Engineering, 2015;* ***18****:1704.*

[31] BOILEAU E, NITHIARASU P, BLANCO PJ, MÜLLER LO, FOSSAN FE, HELLEVIK LR, DONDERS WP, HUBERTS W, WILLEMET M, ALASTRUEY J. *A benchmark study of numerical schemes for one-dimensional arterial blood flow modelling. International Journal For Numerical Methods In Biomedical Engineering, 2015; e02732.*

[32] ALASTRUEY J, PARKER KH, SHERWIN SJ. *Arterial pulse wave haemodynamics. In 11th International Conference on Pressure Surges, Anderson S (ed). Virtual PiE Led t/a BHR Group, Portugal, 2012; 401-442.*

[33] KROON W, HUBERTS W, BOSBOOM M, VAN DE VOSSE F. *A numerical method of reduced complexity for simulating vascular hemodynamics using coupled 0D lumped and 1D wave propagation models. Computational and Mathematical Methods in Medicine, 2012;* ***2012****(Article ID:156094), 10 pages. DOI: 10.1155/2012/156094.*

[34] ZIENKIEWICZ OC, TAYLOR RL, ZHU JZ. *Finite Element Method: Its Basis and Fundamentals (6th Edition). Butterworth-Heinemann 2005.*

[35] DELESTRE O, LAGRÈE PY. *A 'well-balanced' finite volume scheme for blood flow simulation. International Journal For Numerical Methods In Fluids 2013.* ***72****:177-205. DOI: 10.1002/fld.3736*

[36] ALASTRUEY J, PASSERINI T, FORMAGGIA L, PEIR J. *Physical determining factors of the arterial pulse waveform: theoretical analysis and estimation using the 1-D formulation. Journal of Engineering Mathematics 2012; 77:1937.*

[37] XIAO N, ALASTRUEY J, FIGUEROA C. *A systematic comparison between 1-D and 3-D hemodynamics in compliant arterial models. International Journal of Numerical Methods in Biomedical Engineering 2014; 30:204231.*

[38] MATTHYS K, ALASTRUEY J, PEIR J, KHIR A, SEGERS P, VERDONCK P, PARKER K, SHERWIN S. *Pulse wave propagation in a model human arterial network: assessment of 1-D numerical simulations against in vitro measurements. Journal of Biomechanics 2007; 40:34763486.*